Valence band structure, edge states, and interband absorption in quantum-well wires in high magnetic fields

G. Goldoni
Departement Natuurkunde, Universiteit Antwerpen (UIA), Universiteitsplein 1, B-2610 Antwerpen, Belgium and Istituto Nazionale Fisica della Materia, Dipartimento di Fisica, Università di Modena, Via Campi 213/A, I-41100 Modena, Italy

A. Fasolino
Istituto Nazionale Fisica della Materia, Dipartimento di Fisica, Università di Modena, Via Campi 213/A, I-41100 Modena, Italy

(Received 3 April 1995; revised manuscript received 10 July 1995)

We present a theoretical study of the magnetic band structure of conduction and valence states in quantum-well wires in high magnetic fields. We show that hole mixing results in a very complex behavior of valence edge states with respect to conduction states, a fact which is likely to be important in magnetotransport in the quantum Hall regime. We show how the transition from one-dimensional subbands to edge states and to Landau levels can be followed by optical experiments by choosing the appropriate, linear or circular, polarization of the light, yielding information on the one-dimensional confinement.

INTRODUCTION

Quasi-one-dimensional (Q1D) semiconductor structures are promising systems for the investigation of novel optical and transport properties, as well as for potential technological applications.[1] The nature of *magnetic* states in Q1D structures is of primary importance in the understanding of transport properties, e.g., in the quantum Hall regime. In addition, characterization of the currently challenging growth of these structures and information on the lateral confinement can be gained by use of high magnetic fields; in fact, in Q1D structures, the magnetic field provides an additional tunable confinement length which can range from much larger to much smaller than the lateral dimension of the wires and can therefore be used to characterize the lateral confinement length in these structures.

Optical characterization of Q1D structures provides very detailed information on electronic states; band structure effects, such as the coupling between heavy-hole (HH) and light-hole (LH) valence states, have been shown to affect the interband optical absorption of Q1D and of laterally modulated structures at zero and low magnetic field,[2] giving rise to anisotropic absorption for linearly polarized light.

In this paper we present a theoretical study of the electronic and optical properties up to high magnetic fields of quantum-well wires (QWW's) obtained by lateral etching of a quantum well (QW).[3] The alternative method of growth of Q1D structures by deposition on nonplanar substrates is also used to achieve smaller confinement lengths.[4,5] In QWW's, electronic states have either a quasi-2D (Q2D) or a Q1D character, depending on the size of the additional lateral confinement with respect to the underlying QW.

As mentioned above, theoretical[2,6] and experimental[5,7–9] investigations have shown that, at zero and low magnetic field, the in-plane anisotropy induced by 1D quantization can be probed by linearly polarized interband spectroscopy. Here we show that, in high magnetic fields, instead, the anisotropic absorption for circularly polarized light of different helicity is more appropriate to study the features resulting from the field-induced hole mixing; A comparison of linearly and circularly polarized light absorption as a function of the field directly probes the lateral potential by monitoring the transition from the low field regime, dominated by 1D confinement, to the high field regime, dominated by Landau quantization.

In Sec. I we outline the method of calculation of conduction and valence states in Q1D structures from zero to high magnetic fields. In Sec. II we focus on the different nature of valence and conduction edge states in QWW's. In Sec. III we present the calculated optical absorption spectra in linearly and circularly polarized light. Finally, summary and conclusions are given in the last section.

I. METHOD

We consider a QWW such as shown in Fig. 1, which we model by a (001)-grown QW, of length d_z, and a lateral infinite square well along (100), of length d_x. In the following we call $V^e(z)$, and $V^h(z)$ the QW confining potential for electrons and holes, respectively, and $V(x)$ the infinite well potential acting laterally on both electrons and holes. We will also consider this system in the presence of a magnetic field B directed along the (001) direction. Previous calculations of hole states in $B \neq 0$ have considered weak sinusoidal potentials, which allow a simpler

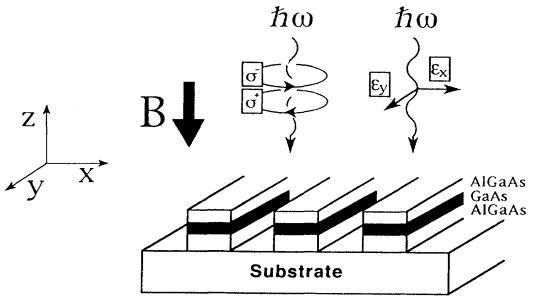

FIG. 1. Sketch of the rectangular QWW's considered here. We assume infinite potential barriers for the lateral well in the x direction. The direction of the magnetic field, as well as the configuration for optical interband absorption with circularly and linearly polarized light, are also indicated.

analytical approach.[2] For both the $B=0$ and $B\neq 0$ cases we will also calculate the oscillator strength for dipolar interband transitions for linearly and circularly polarized light perpendicular to the layers, as illustrated in Fig. 1. As we will show below, the assumption of an infinite well in the x direction allows one to reduce the 2D problem to two 1D problems. In other words, it allows one to factorize the electron envelope function $\Psi^e(\mathbf{r})$ into the product of the envelope functions of the QW bound states $\psi^e(z)$ times the envelope functions $\phi(x)$ of the lateral potential $V(x)$, also in the presence of a magnetic field. Furthermore, the same factorization applied to the uncoupled HH and LH states serves as a suitable representation to include the hole mixing. Conversely, the choice of a QW profile in the z direction can be easily extended to more complex potential profiles, such as coupled QW's.

We obtain the electron and hole energy levels and envelope functions by solving separately the effective-mass electron and hole Hamiltonians.

A. Case $B = 0$

In zero field the effective-mass electron Hamiltonian reads

$$H^e = -\frac{\hbar^2}{2}\frac{\partial}{\partial z}\frac{1}{m^*(z)}\frac{\partial}{\partial z} + \frac{\hbar^2}{2m^*(z)}\left[-\frac{\partial^2}{\partial x^2} + k_y^2\right] + V(x) + V^e(z), \tag{1}$$

where $m^*(z)$ is the bulk conduction electron effective mass which depends on the material and, therefore, on the z coordinate; the usual current-conserving kinetic operator[10] has been used accordingly. We neglect nonparabolicity effects.

The hole Hamiltonian is

$$\mathbf{H}^h = \begin{array}{c} \begin{matrix} +3/2 & -1/2 & +1/2 & -3/2 \end{matrix} \\ \begin{pmatrix} H_h & c_+ & b_+ & 0 \\ c_- & H_l & 0 & -b_+ \\ b_- & 0 & H_l & c_+ \\ 0 & -b_- & c_- & H_h \end{pmatrix} \end{array} + \left[V(x) + V^h(z)\right]\mathbf{I}_4, \tag{2}$$

with

$$H_h = \frac{\hbar^2}{2m_0}\left[(\gamma_1+\gamma_2)\left(\frac{\partial^2}{\partial x^2} - k_y^2\right) + \frac{\partial}{\partial z}(\gamma_1 - 2\gamma_2)\frac{\partial}{\partial z}\right], \tag{3a}$$

$$H_l = \frac{\hbar^2}{2m_0}\left[(\gamma_1-\gamma_2)\left(\frac{\partial^2}{\partial x^2} - k_y^2\right) + \frac{\partial}{\partial z}(\gamma_1 + 2\gamma_2)\frac{\partial}{\partial z}\right], \tag{3b}$$

$$c_\pm = -\sqrt{3}\frac{\hbar^2}{2m_0}\left[\gamma_2\left(\frac{\partial^2}{\partial x^2} + k_y^2\right) \pm 2\gamma_3 k_y \frac{\partial}{\partial x}\right], \tag{3c}$$

$$b_\pm = -\sqrt{3}\frac{\hbar^2}{2m_0}\left(\frac{\partial}{\partial x} \pm k_y\right)\left(\gamma_3\frac{\partial}{\partial z} + \frac{\partial}{\partial z}\gamma_3\right), \tag{3d}$$

where m_0 is the free-electron mass, γ_1, γ_2, and γ_3 are the Luttinger parameters, and $\mathbf{I}_4$ is the identity 4×4 matrix. Equation (2) is obtained from the Luttinger Hamiltonian[11] written in the basis of the eigenstates of the $J = 3/2$ total angular momentum,

$$\left|\frac{3}{2},+\frac{3}{2}\right\rangle, \left|\frac{3}{2},-\frac{1}{2}\right\rangle, \left|\frac{3}{2},+\frac{1}{2}\right\rangle, \left|\frac{3}{2},-\frac{3}{2}\right\rangle, \tag{4}$$

after the substitutions $k_x \to -i\partial/\partial x, k_z \to -i\partial/\partial z$, and symmetrization of the noncommuting products[12] between $\partial/\partial z$ and the z-dependent γ_i's.

The eigenstates of H^e can be factorized as $\Psi^e_{n,m}(\mathbf{r}) = e^{ik_y y}\phi_m(x)\psi^e_n(z)$, where n labels the bound states of the QW potential $V^e(z)$, and m the analytical solutions of the infinite well $V(x)$. Consequently, the eigenvalues of (1) depend quadratically on the in-wire momentum k_y. The solution of the valence states is more complex because the off-diagonal terms in $\mathbf{H}^h$ couple the solutions of the diagonal, electronlike terms H_h and H_l. Following Bockelmann and Bastard,[2] we first solve the electronlike HH and LH Hamiltonians, $H_h + V^h(z) + V(x)$ and $H_l + V^h(z) + V(x)$, giving the factorized solutions $\Psi^{\mathrm{HH}}_{n_h,m} = e^{ik_y y}\psi^{\mathrm{HH}}_{n_h}(z)\phi_m(x)$ and $\Psi^{\mathrm{LH}}_{n_l,m} = e^{ik_y y}\psi^{\mathrm{LH}}_{n_l}(z)\phi_m(x)$, where n_h and n_l label the HH and LH states. Then we expand the solution of the hole Hamiltonian $\mathbf{H}^h$ onto the following basis set:

$$|\mathrm{HH}^+; n_h, m\rangle = (\Psi^{\mathrm{HH}}_{n_h,m}, 0, 0, 0), \tag{5a}$$

$$|\mathrm{LH}^-; n_l, m\rangle = (0, \Psi^{\mathrm{LH}}_{n_l,m}, 0, 0), \tag{5b}$$

$$|\mathrm{LH}^+; n_l, m\rangle = (0, 0, \Psi^{\mathrm{LH}}_{n_l,m}, 0), \tag{5c}$$

$$|\mathrm{HH}^-; n_h, m\rangle = (0, 0, 0, \Psi^{\mathrm{HH}}_{n_h,m}). \tag{5d}$$

In the expansion, we let n_h and n_l run over all N_h bound HH and N_l bound LH states of $V^h(z)$, while m runs over M eigenstates of $V(x)$ (typically we take $M = 15$). Finally, we diagonalize the resulting $2\times(N_h+N_l)\times M$ Hamiltonian. Due to the off-diagonal couplings, therefore, the valence band states cannot be assigned to a single set of indices (n,m), in contrast to conduction electrons; this mixing results in a strongly nonparabolic in-wire energy dispersion.

When we diagonalize the hole Hamiltonian $\mathbf{H}^h$, we do not make the axial approximation, as assumed in Ref. 2, which is more severe in QWW's than in QW's, as shown later in Sec. III.

B. Case $B \neq 0$

When we include a uniform magnetic field $\boldsymbol{B} = (0,0,B)$ along the QW growth direction, described by the vector potential $\boldsymbol{A} = (0, Bx, 0)$, the electron Hamiltonian H^e, neglecting the electron spin splitting, reads

$$-\frac{\hbar^2}{2}\frac{\partial}{\partial z}\frac{1}{m^*(z)}\frac{\partial}{\partial z} + \frac{1}{m^*(z)/m_0}\left[-\frac{\hbar^2}{2m_0}\frac{\partial^2}{\partial x^2} + \frac{m_0\omega^2}{2}(x-x_0)^2\right] + V^e(z) + V(x) \quad (6)$$

and the hole Hamiltonian becomes

$$\mathbf{H}^h - 2\kappa\mu_B B \mathbf{J}_z\,, \quad (7)$$

where $\mathbf{H}^h$ is given by (2) with

$$H_h = (\gamma_1+\gamma_2)\left[\frac{\hbar^2}{2m_0}\frac{\partial^2}{\partial x^2} - \frac{m_0\omega^2}{2}(x-x_0)^2\right] + \frac{\hbar^2}{2m_0}\frac{\partial}{\partial z}(\gamma_1-2\gamma_2)\frac{\partial}{\partial z} + V^h(z) + V(x)\,, \quad (8a)$$

$$H_l = (\gamma_1-\gamma_2)\left[\frac{\hbar^2}{2m_0}\frac{\partial^2}{\partial x^2} - \frac{m_0\omega^2}{2}(x-x_0)^2\right] + \frac{\hbar^2}{2m_0}\frac{\partial}{\partial z}(\gamma_1+2\gamma_2)\frac{\partial}{\partial z} + V^h(z) + V(x)\,, \quad (8b)$$

$$c_\pm = -\sqrt{3}\left[\gamma_2\left(\frac{\hbar^2}{2m_0}\frac{\partial^2}{\partial x^2} + \frac{m_0\omega^2}{2}(x-x_0)^2\right) \pm \gamma_3\frac{\hbar\omega}{2}\left(1 + 2(x-x_0)\frac{\partial}{\partial x}\right)\right], \quad (8c)$$

$$b_\pm = -\sqrt{3}\left[\frac{\hbar^2}{2m_0}\frac{\partial}{\partial x} \pm \frac{\hbar\omega}{2}(x-x_0)\right]\left(\gamma_3\frac{\partial}{\partial z} + \frac{\partial}{\partial z}\gamma_3\right). \quad (8d)$$

$\mathbf{J}_z$ is the diagonal matrix representing the z component of the angular momentum operator in the basis (4); κ is an additional Luttinger parameter, $\omega = eB/m_0$ is the cyclotron frequency, and $x_0 = -l_m^2 k_y$ is the semiclassical "orbit center," where $l_m = (\hbar/eB)^{1/2}$ is the magnetic length. The hole eigenstate dependence on the in-wire wave vector k_y of the $B = 0$ case is now replaced by the dependence on x_0.

Both for H^e and for the diagonal terms of $\mathbf{H}^h$ the lateral potential in the x direction is, at $B \neq 0$, the sum of the infinite well plus a parabolic effective potential. The latter term is equal for the two Hamiltonians so that, at each B and each x_0, the electron and hole $\phi_m(x)$'s are the same, as in the $B = 0$ case. In high magnetic fields, the $\phi_m(x)$'s reduce to harmonic oscillator eigenstates when x_0 is far from the barrier, i.e., when the confinement along x, due to the parabolic magnetic potential, is not affected by the infinite barriers; instead, when x_0 is near the barriers the $\phi_m(x)$'s are the so-called edge states.[13] In view of the possible application to other confinement potentials, we have found it convenient to compute both the $\psi_n(z)$'s and the $\phi_m(x)$'s numerically by direct integration of the Schrödinger equation in real space.

II. ENERGY LEVELS AND EDGE STATES OF QWW's

In Fig. 2(a) and Fig. 2(b) we show the calculated hole subbands for QWW's formed by a $GaAs/Al_{0.35}Ga_{0.65}As$ QW of width $d_z = 10$ nm and by lateral infinite wells of width $d_x = 30$ nm and $d_x = 100$ nm, respectively. Each HH and LH bound state of the QW is split by the lateral potential into a series of 1D subbands of mixed character. In Table I we give the orbital composition of selected states as compared to the purely HH or LH states of the QW at zero in-plane wave vector. As expected, the addi-

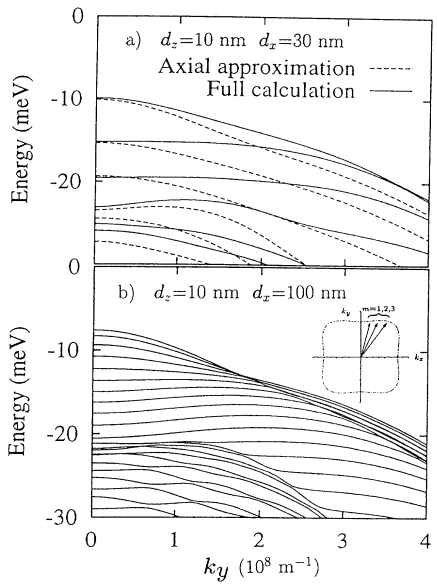

FIG. 2. (a) One-dimensional valence subbands for a $GaAs/Al_{0.35}Ga_{0.65}As$ QWW with d_z=10 nm and d_x=30 nm. Solid line: full inclusion of hole mixing; dashed line: axial approximation. (b) One-dimensional valence subbands for a $GaAs/Al_{0.35}Ga_{0.65}As$ QWW with d_z=10 nm and d_x=100 nm. The inset shows how the warped QW band structure is further quantized by the one-dimensional potential so that each in-wire momentum k_y corresponds to an effective in-plane wave vector $\mathbf{k}_\parallel = (k_x^{\text{eff}}, k_y)$, away from the (010) direction, of the underlying, anisotropic QW band structure.

TABLE I. Comparison of orbital character of the QW bound states and of the QWW levels at $k_y = 0$ having mainly $m = 0$ character at $B = 0$ for the two differently confined QWW's of Fig. 2. For each QWW, we give the energy (in meV) of the lowest level deriving from each pure QW state, the percentage of HH or LH character, and the percentage of $m = 0$ character. The pure QW HH_1, LH_1, and HH_2 levels are further confined by the QWW potential $V(z)$ and acquire a mixed HH-LH character.

	QW $d_x = \infty$	QWW, $d_x = 100$ nm			QWW, $d_x = 30$ nm					
					Full calculation			Axial approximation		
	E	E	HH/LH	$m = 0$	E	HH/LH	$m = 0$	E	HH/LH	$m = 0$
HH_1	-7.39	-7.62	100	100	-9.94	98	98	-10.14	98	99
LH_1	-22.55	-22.52	85	59	-23.06	84	81	-23.41	89	88
HH_2	-29.39	-30.19	85	85	-35.89	67	62	-35.64	63	57

tional confinement energy and hole mixing are much less for $d_x = 100$ nm than for $d_x = 30$ nm. Furthermore, in Fig. 2(a) and Table I we compare the calculated 1D hole subbands with those obtained within the axial approximation for the same structure. The anisotropy-induced couplings have a rather strong effect on the curvature of the subbands; in particular, the electronlike curvature of the light-hole-derived 1D subbands is strongly reduced in the axial approximation. In fact, as sketched in the inset of Fig. 2(b), due to the quantization of the lateral wave vector k_x, each in-wire momentum k_y corresponds to an effective in-plane wave vector $\mathbf{k}_{\|} = (k_x^{\text{eff}}, k_y)$, away from the (010) direction, of the underlying, anisotropic QW band structure.[14] Here $k_x^{\text{eff}} = m\pi/d_x$, where m is the QWW subband index. Therefore, as is apparent in Fig. 2(a), in QWW's not only the in-wire dispersion but also the hole confinement energies are affected by the axial approximation.

In Fig. 3 we show the electron and hole magnetic levels at $B = 10$ T for the same QWW of Fig. 2(b). We plot the magnetic levels as a function of the semiclassical "orbit center" x_0. The most striking effect is that, while the electrons [Fig. 3(a)] display a ladder of edge states with well defined increasing oscillator number,[15] the valence edge states [Fig. 3(b)] have complicated shapes which are likely to be of relevance for magnetotransport, particularly in the integer quantum Hall regime. As for the 1D subbands, also here the axial approximation is very severe.

The comparison of Figs. 3(a) and 3(b) clearly shows that, for holes, the crossover from bulk Landau levels to edge states close to the barrier is less straightforward than for electrons. In fact, each hole state is a mixture of oscillator states of different quantum number m. As a consequence, each component starts experiencing the effect of the barrier at a different value of the magnetic field. As shown in Table II, the second hole level is the only one almost purely $m = 0$ and, indeed, it starts deviating from a flat dispersion at the same x_0 as the $m = 0$ electron state, while all others have a mixed composition resulting in more complicated dispersions.

This point is further clarified by aid of Fig. 4 and Table II. In Fig. 4 we compare the calculated hole magnetic levels for the two QWW's of Fig. 2 ($d_z = 10$ nm and either $d_x = 30$ nm or $d_x = 100$ nm) in a magnetic field of 10 and 30 T. We recall that at $B = 10$ T $l_m \simeq 8$ nm, i.e., comparable to half the thinner d_x, while at $B = 30$ T $l_m \simeq 4.7$ nm, i.e., smaller than half d_x for both structures. Therefore, at $B = 10$ T, for $d_x = 30$ nm [panel 4(a)] all Landau levels are perturbed by the lateral barriers also at the center of the well, while for $d_x = 100$ nm [panel 4(c)] the first edge states evolve to flat Landau levels away from the barrier. Conversely, at $B = 30$ T [panels 4(b) and 4(d)] we find that the energy structure of all edge states down to -40 meV is the same for the two values of d_x and is dominated by Landau quantization, due to the field, rather than by the one-dimensional confinement.

Table II gives a rationale for this behavior. It can be seen that very few states are basically composed of only

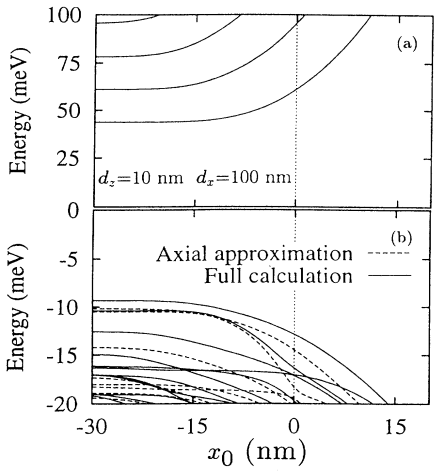

FIG. 3. Conduction (a) and valence (b) edge state energy of a $GaAs/Al_{0.35}Ga_{0.65}As$ QWW with $d_z = 10$ nm and $d_x = 100$ nm at $B = 10$ T as a function of the semiclassical "orbit center" x_0. The origin of energy is at the conduction and valence bulk band edges, respectively. The origin $x_0 = 0$ is chosen to coincide with the infinite barrier edge, indicated by the vertical dotted line, the wire extending from 0 to $-d_x$. Conduction (valence) edge states are bent upward (downward) due to magnetic confinement close to the barrier. Valence edge states calculated with full inclusion of the hole mixing (solid line) are compared with those calculated within the axial approximation (dashed line).

one harmonic oscillator number and that the mixing increases with increasing B. Furthermore, at high fields, the eigenvalues at the center of the well of the low oscillator index levels do not depend any more on the lateral potential. This transition takes place at different values of the magnetic field for each level, as illustrated in Fig. 5. Here we show the evolution of electron and hole states as a function of the field for two values of d_x. The striking difference between electron and hole levels is related to the mixed composition of the hole states, given in Table II. The nontrivial behavior of hole levels in Fig. 5 suggests that the transition from the low field regime, dominated by 1D quantization, to the high field regime, dominated by Landau quantization, is associated with large changes in the wave function composition, with consequent influence on the matrix elements for optical transitions, which we calculate in the next section. Our aim is to show that the transition from the low to the high field regime can be monitored by optical experiments with linearly and circularly polarized light, giving unambiguous information on the lateral confinement.

TABLE II. For different values of d_z, d_x, and B, this table gives, for the lowest subbands, the energy and the HH_1^+, HH_1^-, LH_1^-, and LH_1^+ character at x_0 located at the center of the lateral well. For each component, the main Landau oscillator index is indicated. Notice that at $B = 30$ T the eigenvalues with low oscillator index do not depend on the confining length d_x.

$d_z = 10$ nm, $d_x = 30$ nm, $B = 10$ T									
Band	E (meV)	HH_1^+	m	HH_1^-	m	LH_1^-	m	LH_1^+	m
1	-10.24	0.89	0			0.07	2		
2	-10.69			0.98	0			0.01	2
3	-16.29	0.72	1			0.20	3		
4	-17.50			0.70	1			0.20	1,3
5	-19.35			0.36	2,0			0.54	0,2
6	-19.47	0.03	2			0.82	0		
7	-21.09			0.28	3			0.52	1
8	-23.12	0.53	2			0.36	2,4		
9	-24.01	0.09	3			0.76	1		
10	-25.91			0.09	4			0.78	0,2,4
$d_z = 10$ nm, $d_x = 30$ nm, $B = 30$ T									
Band	E (meV)	HH_1^+	m	HH_1^-	m	LH_1^-	m	LH_1^+	m
1	-11.52	0.77	0			0.17	2		
2	-15.96			0.95	0			0.05	2
3	-19.89	0.02	2			0.85	0		
4	-20.27	0.61	1			0.29	3		
5	-20.27			0.15	3			0.64	1
6	-20.78			0.24	2			0.70	0
7	-27.38			0.23	4			0.64	2
8	-28.42	0.51	2			0.36	4		
9	-29.47			0.58	1			0.25	3
10	-30.50	0.07	3			0.78	1		
$d_z = 10$ nm, $d_x = 100$ nm, $B = 30$ T									
Band	E (meV)	HH_1^+	m	HH_1^-	m	LH_1^-	m	LH_1^+	m
1	-11.56	0.76	0			0.17	2		
2	-15.93			0.95	0			0.05	2
3	-19.87	0.03	2			0.84	0		
4	-20.37			0.15	3			0.64	1
5	-20.41	0.60	1			0.29	3		
6	-20.79			0.24	2			0.70	0
7	-27.42			0.26	4			0.61	2
8	-28.54	0.49	2			0.38	4		
9	-29.37			0.54	1			0.29	3
10	-30.48	0.09	3			0.76	1		

III. OPTICAL ABSORPTION IN QWW's

At B=0, the two in-plane linear polarizations of the light induce different interband absorption probability, as a consequence of the one-dimensionality of the hole states,[2] while the two circular polarizations give the same absorption intensity. At the opposite limit of very large fields, the situation is reversed: we expect the two in-plane linear polarizations to give degenerate spectra, due to the recovered two-dimensional character of hole states, while the two circular polarizations of the light, being coupled to different components of the spin-orbit coupled states, give different spectra. Therefore, in the intermediate regime, we expect large changes in the absorption spectra for both circularly and linearly polarized light, as shown next.

Strictly speaking, a calculation of magneto-optical properties in Q1D structures should include excitonic effects. The exact inclusion of the Coulomb interaction is, however, a complicated task in itself and theoretical calculations exist only for model, purely 1D structures in zero field.[16] However, several studies[17,18] have shown that, in Q2D structures, a perturbative excitonic correction[19] added to the one-particle absorption spectra yields a good description of magneto-optical experiments in the high field regime, provided the hole mixing is included. Therefore we expect our results, obtained in a one-particle approximation, to be qualitatively correct, particularly in the high field regime close to the transition to 2D behavior.

In Fig. 6, we compare the calculated optical absorption spectra for linear and circular light polarization at $B =$ 10 T and $B = 30$ T and for $d_x = 30$ nm; we have labeled the main features according to the orbital character of the initial (hole) and final (electron) states involved in the transitions. The mixing of hole states causes the fact that very many hole levels have nonvanishing oscillator strength for the transition to the same electron state, making the spectra rich and informative. For instance, at 10 T the transition $LH_{10}^- \rightarrow e_{10}^{\downarrow}$, which is induced by σ^+ polarized light, gives rise to a single peak in the spectra, while the transition $LH_{10}^+ \rightarrow e_{10}^{\uparrow}$ is split into three peaks in σ^- polarization. In fact, as shown in Table II, there is only one level (level 6) with strong LH^- character and a strong $m = 0$ component, while there are three levels with LH^+ and $m = 0$ character (levels 5, 10, and a deeper one which is not reported in the table).

Figure 6 shows that, while the spectra for light linearly

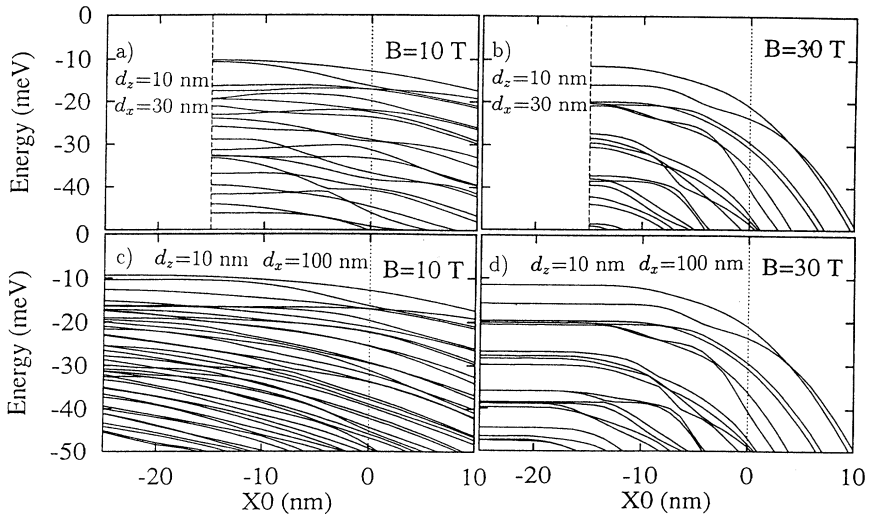

FIG. 4. Valence edge states of $GaAs/Al_{0.35}Ga_{0.65}As$ QWW's with d_z = 10 nm: (a) d_x = 30 nm, B = 10 T; (b) d_x = 30 nm, B = 30 T; (c) d_x = 100 nm, B = 10 T; (d) d_x = 100 nm, B = 30 T. x_0 = 0 is set at the position of the right-hand infinite barrier, indicated by vertical dotted lines. Vertical dashed lines in panels (a) and (b) indicate the wire center; the edge states are symmetric with respect to the wire center. Notice that, at B = 30 T, the edge states of the two samples have become identical down to ~ -40 meV.

polarized along the two in-plane directions of the QWW become very similar at high fields, as we expect from the isotropic character of the orbital motion, large differences are present in the spectra calculated for the two circular polarization of the light, as observed in Q2D structures.[17] Hence, these differences can be regarded as a fingerprint of the transition from 1D dynamics to Landau quantization; by studying the evolution of the linear and circular absorption, the transition from the low field to the high field regime can be followed, yielding quantitative information on the effective length of the 1D confinement.

Figure 7 shows how the anisotropy between spectra obtained from linearly polarized light decreases as a function of the field. Calculations are performed for the same sample of Fig. 6. The anisotropy is expressed as $100 \times (I_x - I_y)/(I_x + I_y)$, where I_x and I_y are the heights of the lowest energy peak of the absorption spectra calculated for the x and y polarizations, respectively. As expected from the above discussion, the anisotropy is strongly quenched by the field and decreases monotonically from 10% at B = 0 to 3% at B = 20 T for this sample. At fields larger than 20 T, this peak splits into a double peak, as shown in Fig. 6 at 30 T, and the above definition does not apply.

Finally, in Fig. 8 we show the evolution of the calculated spectra for the two circular polarizations of the light as a function of magnetic field for the d_z = 10 nm, d_x = 30 nm sample. Hole mixing is responsible for the complex features in the low energy range, which could hopefully be experimentally detected. In Fig. 8 the calculated spectra for the σ^- polarization show a clear anticrossing behavior around 1590 meV. This feature, which is due to HH-LH mixing and would be absent in a simple, uncoupled-hole model, can be seen, again, as a fingerprint of the transition from 1D subbands to Landau levels of hole states. Note that this anticrossing is totally absent in the corresponding peaks for the σ^+ polarization, as a consequence of the smaller mixing of HH^- and LH^- states as compared to HH^+ and LH^+ states (see Table II).

CONCLUSIONS

We have presented a study of the electronic structure of rectangular QWW's following the transition from the 1D quantization at zero magnetic fields of the subband structure to Landau quantization at high magnetic fields.

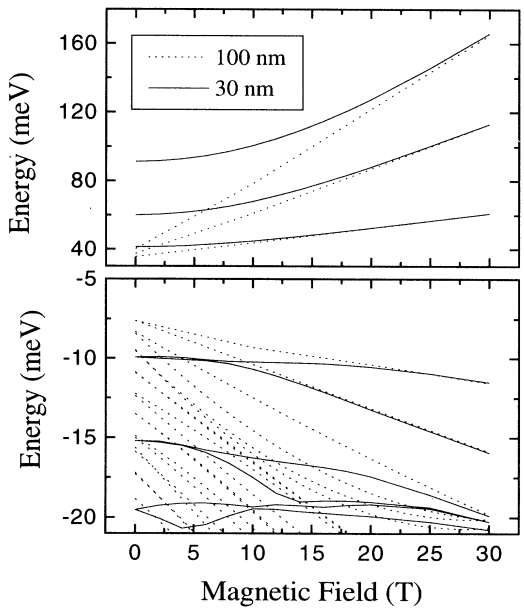

FIG. 5. Top panel: shift of the conduction edge states calculated at the wire center as a function of the magnetic field for d_x = 30 nm (solid line) and d_x = 100 nm (dashed line). Conduction edge states subsequently converge to the bulk value. Bottom panel: shift of the valence edge states calculated at the wire center as a function of the magnetic field for d_x = 30 nm (solid line) and d_x = 100 nm (dashed line). The origin of energy is at the conduction and valence bulk band edges, respectively. Notice that, in contrast to electrons, the convergence to bulk energies does not occur in a regular fashion for holes.

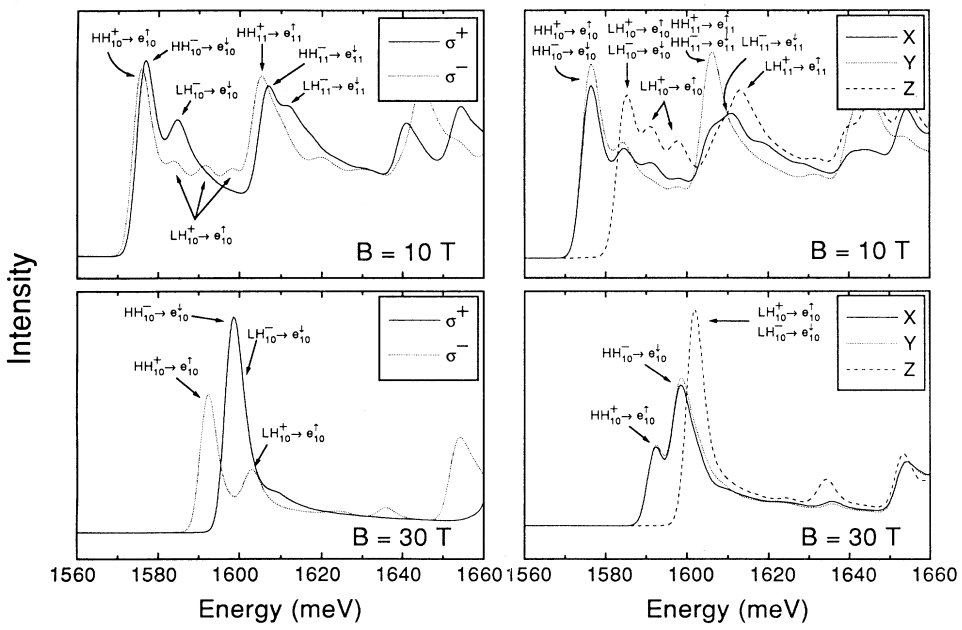

FIG. 6. Calculated optical absorption spectra of a GaAs/$Al_{0.35}Ga_{0.65}As$ QWW with d_z=10 nm and d_x=30 nm for linear (X, Y, Z) and circular (σ^+, σ^-) light polarization at B = 10 T and B = 30 T, as indicated in each panel. Calculated spectra have been convoluted with a 5 meV Gaussian broadening. We have labeled the main transitions *initial state* → *final state*, where the initial valence state is labeled according to its main component ($HH^{\pm}_{nm}$ or $LH^{\pm}_{nm}$) and the final electronic state is labeled as $e^{\uparrow\downarrow}_{nm}$.

We have focused on the behavior of the spin-orbit coupled valence band, and, to this purpose, we have developed a method of solution of the Luttinger Hamiltonian for Q1D structures at both B=0 and $B \neq 0$. We have shown that the hole mixing gives rise to a rather complex edge state structure compared to electron states. Furthermore, we have shown that a study of the optical interband transition for linearly and circularly polarized light could be used to get information on the lateral confinement. As we discussed in Sec. III, excitonic effects, which are neglected in the present calculations, should not change our results qualitatively, particularly in the regime of high fields. Furthermore, the present one-particle calculation, which takes into account the coupled nature of the valence subbands, is a necessary ingredient for a successive calculation of the magnetoexciton.

This study is also preliminary to a study of more complex Q1D structures[4,5] showing very promising optical properties. In these structures, the two confinement directions are of comparable width and have potential barriers of the same height and, therefore, should be treated on the same footing. Theoretical investigations of valence states in these structures are currently in progress. We hope that the present work will stimulate further experimental and theoretical work on both the transport and optical properties of these interesting systems.

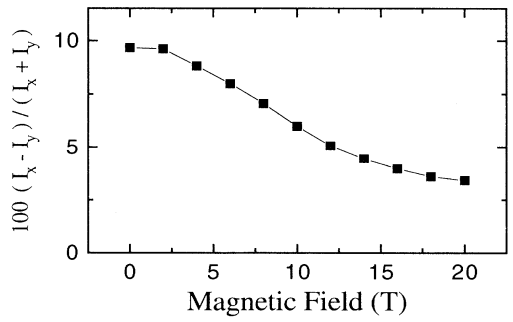

FIG. 7. Anisotropy of the calculated absorption spectra with linearly polarized light as a function of the magnetic field and for the sample of Fig. 6. I_x and I_y are defined in Sec. III.

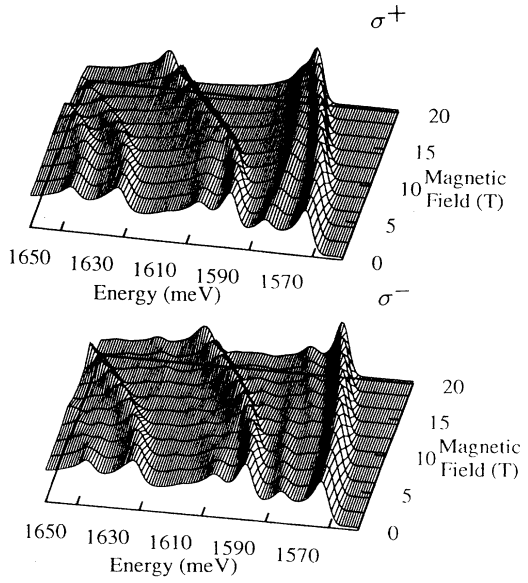

FIG. 8. Calculated optical absorption spectra of a GaAs/$Al_{0.35}Ga_{0.65}As$ QWW with d_z = 10 nm and d_x = 30 nm for the two circular polarizations of the light. Notice the avoided crossing around $E \sim$ 1590 meV for σ^-, absent in the σ^+ polarization.

ACKNOWLEDGMENTS

We thank F. Rossi for fruitful discussions. We acknowledge the project ESPRIT 7260 (SOLDES) for partial financial support. Part of this work has been carried out within the European Human Capital & Mobility Network magNET, No. ERBCHRXCT 920062.

[1] For a recent review see, e.g., R. Cingolani and R. Rinaldi, Riv. Nuovo Cimento **16**, 1 (1993).
[2] U. Bockelmann and G. Bastard, Phys. Rev. B **45**, 1688 (1992); **45**, 1700 (1992).
[3] See, e.g., J. Y. Marzin, A. Izrael, and L. Birotheau, Solid State Electron. **37**, 1091 (1994), and Ref. 7.
[4] M. Walther, E. Kapon, C. Caneau, D. M. Hwang, and L. M. Schiavone, Appl. Phys. Lett. **62**, 2170 (1993).
[5] R. Rinaldi, R. Cingolani, M. Lepore, M. Ferrara, I. M. Catalano, F. Rossi, L. Rota, E. Molinari, P. Lugli, U. Marti, D. Martin, F. Morier-Gemoud, P. Ruterana, and F. K. Reinhart, Phys. Rev. Lett. **73**, 2899 (1994); R. Rinaldi, M. Ferrara, R. Cingolani, U. Marti, D. Martin, F. Morier-Gemoud, P. Ruterana, and F. K. Reinhart, Phys. Rev. B **50**, 11 795 (1994).
[6] D.S. Citrin and Y.-C. Chang, Phys. Rev. B **43**, 11 703 (1992).
[7] M. Kohl, D. Heitman, P. Granbow, and K. Ploog, Phys. Rev. Lett. **63**, 2124 (1989).
[8] M. Tanaka, J. Motohisa, and H. Sakaki, Surf. Sci. **228**, 408 (1990).
[9] M. Notomi, M. Okamoto, H. Iwamura, and T. Tamamura, Appl. Phys. Lett. **62**, 1094 (1993).
[10] D. J. Ben-Daniel and C. B. Duke, Phys. Rev. **152**, 683 (1966).
[11] J. M. Luttinger, Phys. Rev. **102**, 1030 (1956).
[12] G. Bastard, *Wave Mechanics Applied to Semiconductor Heterostructures* (Les Éditions des Physique, Les Ulis, Paris, 1988).
[13] A. H. MacDonald and P. Streda, Phys. Rev. B **29**, 1616 (1984).
[14] M. Altarelli, U. Ekenberg, and A. Fasolino, Phys. Rev. B **32**, 5138 (1985).
[15] M. Buttiker, Phys. Rev. B **38**, 9375 (1988).
[16] T. Ogawa and T. Takagehara, Phys. Rev. B **43**, 14 325 (1991); **44**, 8138 (1992).
[17] F. Ancilotto, A. Fasolino, and J. C. Maan, Phys. Rev. B **38**, 1788 (1988).
[18] G. Goldoni, T. Ruf, V. F. Sapega, A. Fainstein, and M. Cardona, Phys. Rev. B **51**, 14 542 (1995).
[19] O. Akimoto and H. Hasegawa, J. Phys. Soc. Jpn. **22**, 181 (1967).